Nuclear Instruments and Methods in Physics Research A 601 (2009) 364–371

Contents lists available at ScienceDirect

Nuclear Instruments and Methods in Physics Research A

journal homepage: www.elsevier.com/locate/nima

On site calibration for new fluorescence detectors of the telescope array experiment

H. Tokuno [a,*], Y. Murano [b], S. Kawana [c], Y. Tameda [b], A. Taketa [a], D. Ikeda [a], S. Udo [a,1], S. Ogio [d], M. Fukushima [a], R. Azuma [b], M. Fukuda [b], N. Inoue [c], K. Kadota [e], F. Kakimoto [b], H. Sagawa [a], N. Sakurai [a], T. Shibata [a], M. Takeda [a], Y. Tsunesada [b]

[a] Institute for Cosmic Ray Research, University of Tokyo, Kashiwa, Chiba 277-8582, Japan
[b] Graduate School of Science and Engineering, Tokyo Institute of Technology, Meguro, Tokyo 152-8551, Japan
[c] Graduate School of Science and Engineering, Saitama University, Saitama 338-8570, Japan
[d] Graduate School of Science, Osaka City University, Sumiyoshi, Osaka 558-8585, Japan
[e] Faculty of Knowledge Engineering, Musashi Institute of Technology, Setagaya, Tokyo 158-8557, Japan

ARTICLE INFO

Article history:
Received 25 December 2008
Accepted 27 December 2008
Available online 17 January 2009

Keywords:
Ultra-high energy cosmic rays
Extensive air showers
Fluorescence light

ABSTRACT

The Telescope Array experiment is searching for the origin of ultra-high energy cosmic rays using a ground array of particle detectors and three fluorescence telescope stations. The precise calibration of the fluorescence detectors is important for small systematic errors in shower reconstruction. This paper details the process of calibrating cameras for two of the fluorescence telescope stations. This paper provides the operational results of these camera calibrations.

1. Introduction

In 1966 Greisen, Zatsepin, and Kuzmin predicted that the energy spectrum of ultra-high energy cosmic rays (UHECRs) will have a cutoff [1]. Detailed measurement of the UHECR flux in the GZK cutoff region is important when studying the origin and propagation of UHECRs. Currently, the energy spectra of UHECRs have been reported by Volcano Ranch, Suger, Haverah Park, Yakutsk, Fly's Eye, HiRes, Akeno, AGASA, and Pierre Auger [2–10]. The energy spectra around 10^{19} eV have been obtained with small statistical error [7–10]. However, these energy spectra are not consistent. These inconsistencies can be explained by including the estimated systematic error. Accordingly, the degree of systematic error is comparable to the difference between energy spectra. In order to obtain a definitive UHECR energy spectrum, a new experiment is needed with small systematic and statistical error.

In order to take detailed measurements of the northern hemisphere UHECR flux, we have constructed the Telescope Array (TA) in Utah, USA [11]. This experiment has a hybrid detector, which consists of a surface detector (SD) array and fluorescence detectors (FDs). The SD array measures extensive air shower (EAS) particles on the ground while FDs detect air fluorescence photons induced by EAS particles.

Each SD has two 1.2 cm thick layers of 3 m^2 plastic scintillator. The SD array consists of 507 SDs with 1.2 km spacing covering a total 700 km^2. This is seven times larger than the AGASA array. The expected trigger efficiency from our simulation studies is 100% for primary protons with energies above 10^{19} eV and zenith angles within 45° [12].

The three FD stations (known as BR, LR, and MD) have been installed surrounding the SD array. BR is located at the southeast corner of the SD array while LR is to the southwest. Both stations are new detectors designed specifically for the TA experiment. Each station has 12 telescopes. MD is located at the northeast corner of the array and has 14 telescopes [13]. The MD telescopes consist of the cameras and electronics formerly used in the HiRes-I experiment and the mirrors from the HiRes-II experiment.

In the TA experiment, the SD array and the FDs observe EASs independently. Events measured by both SD array and FDs provide crucial data in studying the systematic differences of the reconstructed shower parameters. Our FDs are operated on moonless clear nights. Accordingly, the expected duty factor of FDs is about 10%, whereas that of SD is almost 100%. From our simulation studies, expected FD's stereo detection area is 1000 km^2 for primary protons with energies above 10^{19} eV and zenith angles below 45° [14]. Thus, this expected observation area covers the whole area of the SD array. The expected observation

*Corresponding author. Tel.: +81 4 7136 5153; fax: +81 4 7136 3134.
E-mail address: htokuno@icrr.u-tokyo.ac.jp (H. Tokuno).
[1] Present address: Faculty of Engineering, Kanagawa University, Yokohama, Kanagawa 221-8686, Japan.

0168-9002/$ - see front matter © 2009 Elsevier B.V. All rights reserved.
doi:10.1016/j.nima.2008.12.210

efficiency of the SD array is 100% for the same air showers. Therefore, the showers with primary energies above 10^{19} eV are measured by SD and are simultaneously observed by multiple FDs. Using these events we estimate the systematic error of the fluorescence (HiRes type) and the surface (AGASA type) detectors. The expected detection rate of these events is 70 events/year for primary energies above 10^{19} eV [14].

For shower reconstructions to have small systematic error, the precise calibration of FDs is important. For this purpose, we have developed the following calibration systems [15–18]: (a) absolute calibrations of PMT gains including temperature dependence, (b) monitoring of absolute PMT gains using alpha-ray light sources, (c) adjusting and monitoring of relative PMT gains, (d) response uniformity on the photo cathode for every PMT, (e) end to end detector calibration including the fluorescence yield, (f) measurement of the reflectivities, the focal lengths and the blurs of images of segment mirrors and the combined mirrors, and (g) monitoring of the atmospheric transparency.

In this paper we describe the calibration of (c) and (d) in the BR and LR stations. The brief descriptions of other calibrations are in the previous papers [15–18]. The details will be provided in forthcoming publications. In Section 2, we introduce the PMT cameras in the BR and LR stations. A method for the absolute calibration of PMTs is briefly reviewed in Section 3. We show the results of the calibration of relative PMT gains and the measurement of uniformities of PMT responses in Sections 4 and 5, respectively. In Section 6, we summarize this paper.

2. FDs of the TA experiment

Each FD telescope consists of a spherical mirror, a PMT camera, and readout electronics. Fig. 1 shows a cross-sectional view of a station. Our 3 m aperture spherical mirror consists of 18 segment mirrors, each of which has a hexagonal shape, opposite side distance of 660 mm, and a curvature radius of 6067 mm. The camera has $16 \times 16 (= 256)$ PMTs and is mounted at the prime focus of the mirror. The sensitive area of a camera is 860 mm $\times$ 992 mm, corresponding to a field of view (FOV) of 15° in elevation $\times 18^\circ$ in azimuth. Each camera views a different area of the sky above the SD array, but overlaps its FOV with its neighbors. In total, the FOV of a station is $3^\circ - 33^\circ$ in elevation and 108° in azimuth.

For dust control, we use a UV-transparent acrylic panel (PARAGLAS-UV00 by KURARAY Co. Ltd.) for the front window of the cameras. Fig. 2 shows the typical spectral transmittance of this window measured with a HITACHI-U-1100 spectrophotometer. In addition to these manufacturer specifications, we measured the transmittance for the camera windows on site by comparing the differences between PMT outputs for a stable light source with the windows opened to those with windows closed. The light

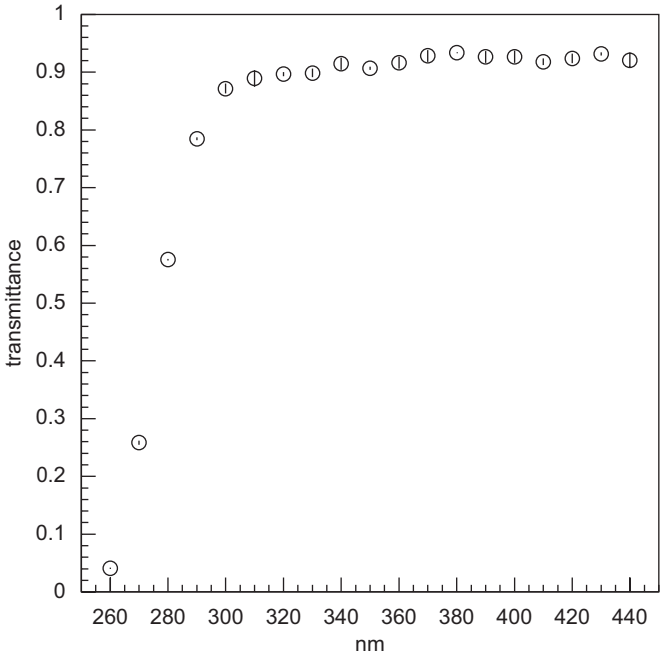

Fig. 2. The typical transmittance of the acrylic window panel on the FD camera. Open circles are the median value of three measurements. Error bars are the difference between the median value and the other two measurements.

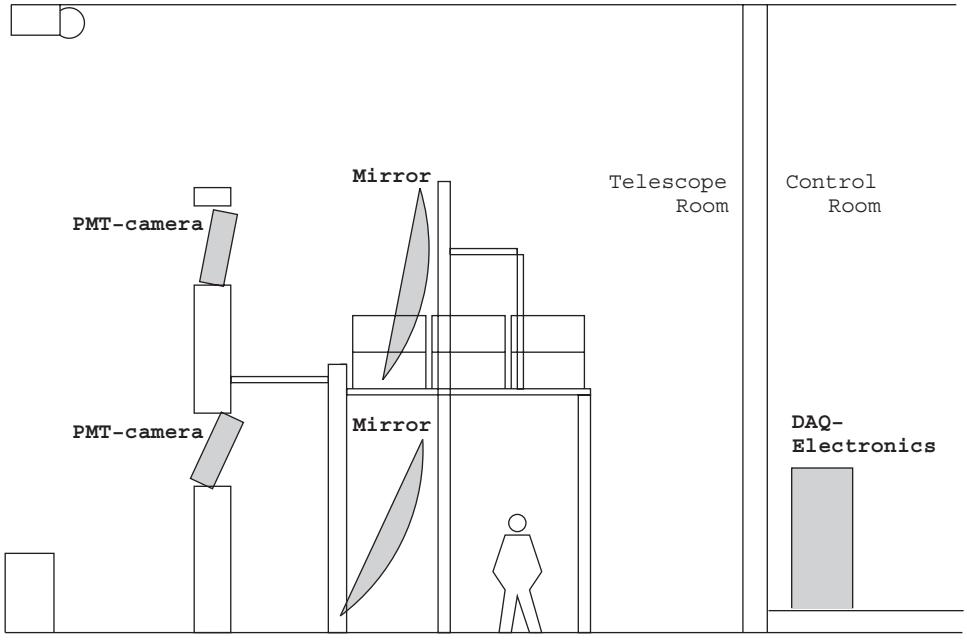

Fig. 1. The cross-sectional view of a fluorescence detector station.

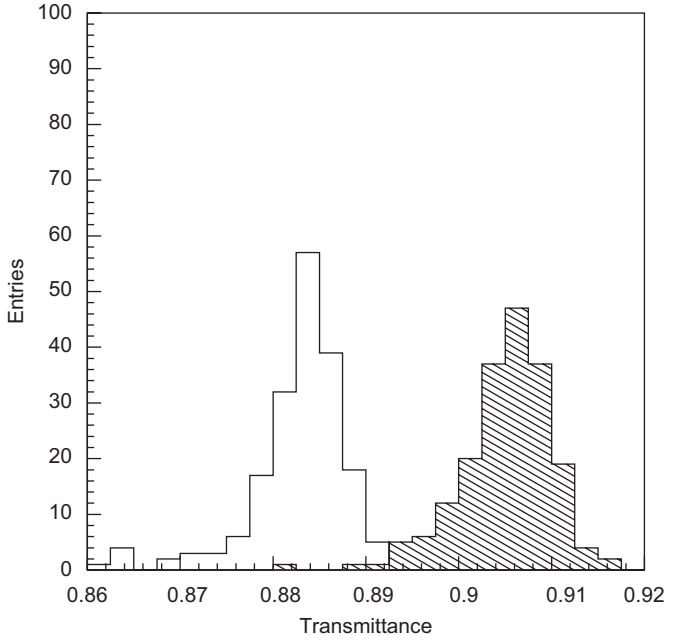

Fig. 3. The transmittance of the front window of a FD-camera at 360 nm measured at each PMT position. Transmittance of camera #00's window at the BR station (open area) is 89% of the typical value. The mean value for camera #2 at the LR station (shadow area) is different from the typical value.

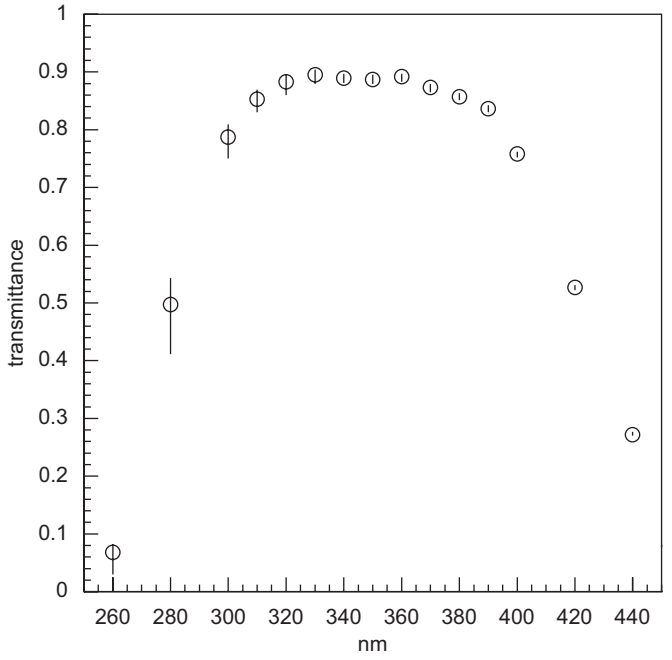

Fig. 4. The typical transmittance of the BG3 filter (number of measurements is 99, error bars: 1σ).

source of this measurement is an Xe flash lamp (HAMAMATSU L4646) loaded with a 360 nm bandpass filter (with bandwidth of 10 nm by Asahi Spectra Inc.). Fig. 3 shows that the individual difference in the transmittance of the windows is smaller than 3% and that the position dependence of the transmittance for each window is smaller than 1%.

Each PMT (HAMAMATSU R9501) has a 2 in. diameter hexagonal photon sensitive area. All of the PMTs have different applied high voltages and are set to have an equal gain of 8×10^4. Moreover, in order to cut night sky back ground light of longer than 400 nm, a UV transparent filter (SCHOTT BG3) with 4 mm thickness is mounted on the photo cathode of every PMT. Fig. 4 shows the spectral transmittance of the filter measured with the spectrophotometer. From our simulation studies, signal to noise ratio will be improved 30% by the filter.

3. Absolute calibration of PMTs

In the laboratory, we measured the relation between a gain and an applied high voltage for three PMTs per camera using an absolute light source. For this measurement, we developed an absolute calibration system called CRAYS (Calibration using RAYleigh Scattering). It consists of an N_2 filled chamber and an N_2 pulse laser (Thermo Laser Science Inc. VSL-337ND-S). The pulse laser has a wavelength of 337.1 nm, an output power of 300 μJ/pulse, and a pulse width of 4 ns. It also has an energy meter (Laser Probe Inc. RjP-435) to monitor the intensity per laser shot with the absolute accuracy of ±5%. On a window of the chamber, a PMT to be calibrated is set to face the light path of laser shot. This path is fixed perpendicular to the line of sight of the PMT. Rayleigh scattered photons illuminated the PMT as a calibration light source. For precise estimations of the number of photons per shot, we monitor: laser shot intensities, the geometry of the experimental setup, gas temperature, and gas pressure. We achieved systematic uncertainty for the intensity estimation to be ±8%. With this CRAYS calibration, we obtained the output

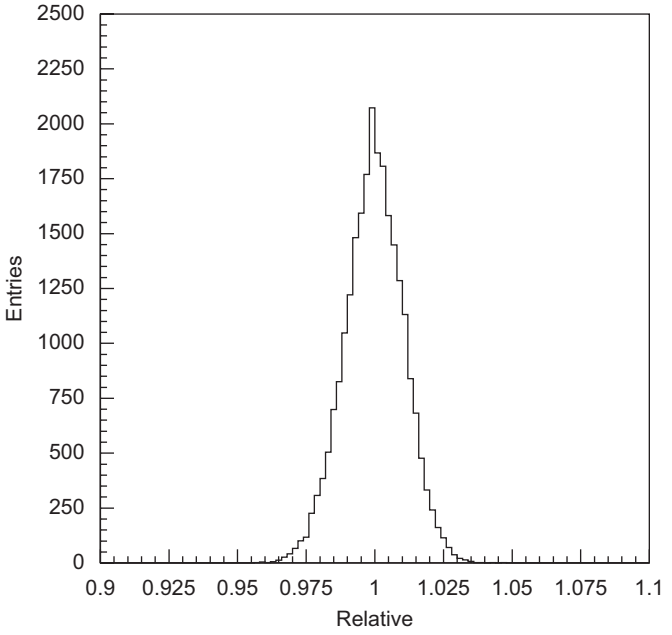

Fig. 5. The typical stability of relative light intensity of Xe flasher.

response of a PMT for 337.1 nm photons. Additionally, our own calibrations and the manufacturer specification separately provide us with the quantum efficiency of the PMTs, the transmittance of the UV filters, and the wavelength dependences of the UV filters. Combining these wavelength dependencies with the CRAYS calibrations, we obtain a PMT output response function for any given wavelength. For more detail on the CRAYS calibration, please refer to the next paper in preparation (also, you can find a brief description in Ref. [15]).

Gains of the absolutely calibrated PMTs are monitored every hour during observations. A tiny light source called YAP is

mounted on the photo cathode of each absolutely calibrated PMT. This light source consists of an $YAlO_3$: Ce scintillator and a 50 Bq alpha ray source of ^{241}Am [19,20]. The shape of YAP is a cylinder with a diameter of 4 mm and a height of 1 mm with the scintillator set on the bottom. The peak wavelength is 370 nm, and the typical full width at half maximum (FWHM) of the light pulses are 20 ns. Since the light intensity per pulse is reduced 40% by a neutral density filter attached on the surface of YAP, the typical intensity measured with a PMT is 450 p.e. with the individual difference of 5% and a fluctuation of 10%. The YAP light source is secured in the center hole of the UV filter with an epoxy resin, EPO-TEK 305, EPOXY TECHNOLOGY. The UV resistance of this epoxy resin has been measured by Kobayashi et al. [21]. From this result we estimate the degradation of transmittance is less than 0.3% per year under our experimental conditions. For every PMT, the photon intensity and its YAP stability is calibrated comparing its intensity with CRAYS.

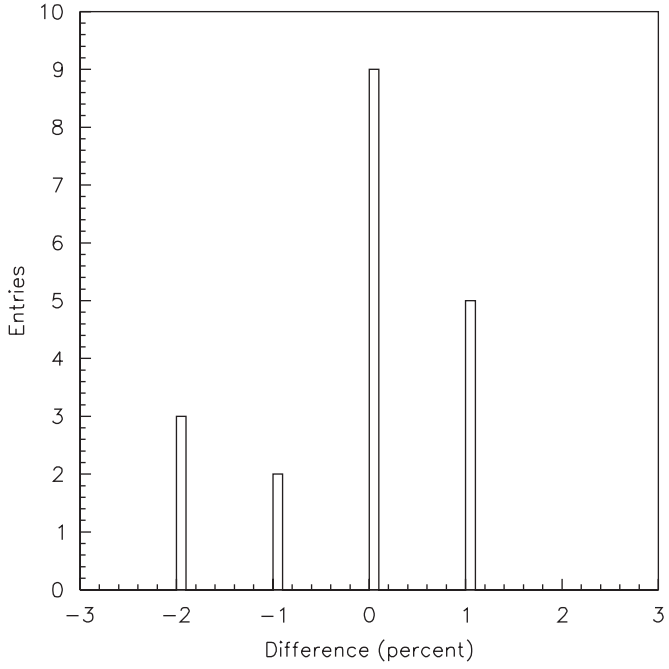

Fig. 6. The differences of the uniformity of Xe flasher from the ray-trace estimations.

4. Relative calibrations of PMTs

The number of absolutely calibrated PMTs is limited, because we can only absolutely calibrate 10 PMTs per day. Therefore, the gains of the un-calibrated PMTs are adjusted to that of the calibrated PMTs in the same camera. For the adjustments we use a light source which illuminates the focal plane with an uniform intensity, and we adjust the applied high voltage of each un-calibrated PMTs until its output is equal to that of the absolutely calibrated PMTs. These adjustments for the PMTs are done several times a year. Currently, this has been done in June, July, August, November 2007, and March 2008. During normal operation periods, we monitor each PMT's deviation from the camera flat response once every hour. This is done using the same light source. Once we obtain gain correction factors from the monitoring data, we can apply them in the analysis scheme.

The light source, called the Xe flasher, consists of an Xe lamp, a power supply, and a 4 mm thick teflon diffuser. The light intensity of one Xe flasher is equivalent to 2×10^4 p.e./PMT per shot. Its typical pulse width is 2 μs FWHM and the typical intensity fluctuation is 1% as shown in Fig. 5. The light source for a camera is mounted on the center of the mirror and is faced to the camera center. Since the diffusion of emitted photons is spherically uniform, the light intensity on the camera surface is highest at the center of the camera. For example, the light intensity on the PMT at the center of the camera is 5% larger than that at a corner of the camera. Geometrical corrections estimated using a ray-trace program are included in the calculations of the gain correction factors.

To confirm the uniformity of Xe flasher emissions, we measured intensity difference and compare it with the ray-trace estimations. The light intensities from an Xe flasher at 19 different points on a camera are measured using the same PMT. Through the measurement, the gain of this PMT is monitored using YAP. The reproducibility of this monitoring is within ±2% at a given point. The measured intensities are consistent with the ray-trace estimations within our ±2% uncertainty (Fig. 6).

While we adjust the PMT gains with an Xe flasher to flat and uniform responses over a camera, we shut off any light from other sources and cover the mirrors with cloths. The high voltages on all the PMTs are adjusted for the camera to have a flat response over the photon sensitive surface within 2% deviation (Fig. 7). As a result, the typical applied high voltage is −880 V (Fig. 8).

The flat responses are monitored during each observation. The major source of PMT gain fluctuations is changing temperature in

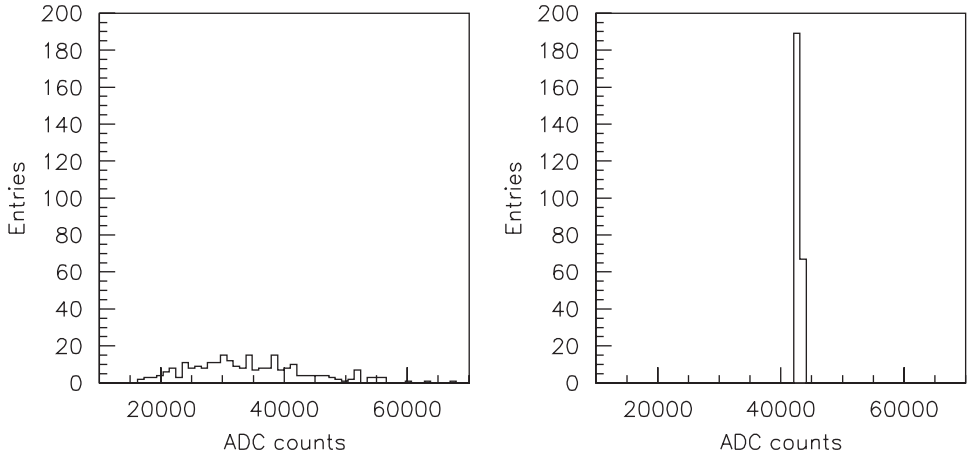

Fig. 7. The left figure is the outputs for a single shot of the Xe flasher when all the PMT were applied the equal high voltage of −850 V. The right is the outputs of PMTs while we adjusted the high voltages. These PMTs are installed in camera #00 at the BR station.

cameras. Therefore, we also monitor temperatures in all the cameras.

From July 2007 to September 2008 the adjusted flat responses for all the cameras are very stable. The standard deviation of the gain instability distribution for all the PMTs is 1%, as shown in Fig. 9. A maximum of 30 PMTs had large deviations, greater than 15%, from the adjusted normal gain. This is 0.5% of the total number of PMTs. Every hour, the measured gain correction factors are used to adjust the PMTs with large deviations. Normally, there are less than four PMTs that are unusable due to gain instabilities. This is less than 0.1% of the total number of the PMTs.

Typically, the gain instabilities are caused by a bad contact between either the signal or high voltage connectors. This, in turn, causes a degradation of the signal to noise ratio.

5. Non-uniformity measurement of the PMT photo cathodes

In general, the quantum and collection efficiencies of a PMT's photo cathode have non-uniformities.

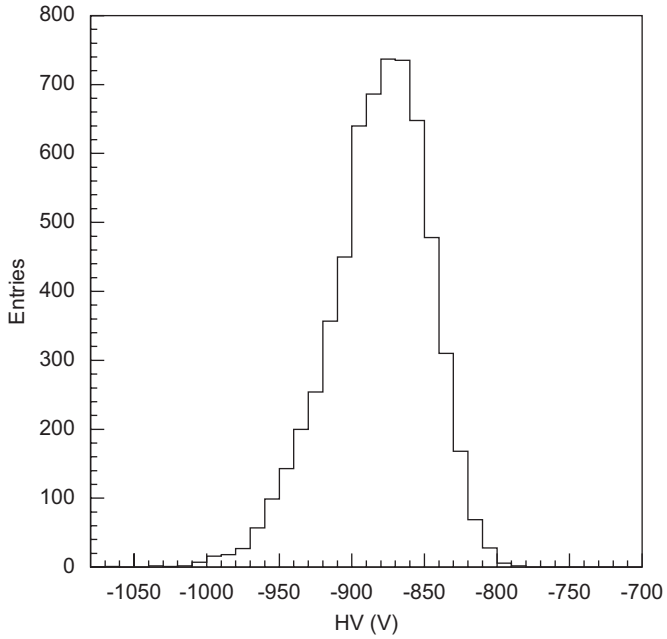

Fig. 8. The adjusted high voltage values for all the PMTs on March 2008.

In our experiment, the averaged response over the whole photo cathode area of each PMT is adjusted using the Xe flashers. Additionally, air fluorescence light partly illuminates the photo cathode of the PMT. The spot size made by air fluorescence light is less than 20 mm at the focal plane. The spot size is defined as the diameter of the circle involving 90% of the reflected photons from parallel incident light. Cathode non-uniformity causes the PMT output to vary if the incident light is non-uniform.

Therefore, the effect of the non-uniformities must be corrected for by precise estimations of the number of incident photons. In order to measure the cathode non-uniformities and make maps of the unresponsive regions between the PMTs, we developed the "XY-scanner". The XY-scanner consists of large XY stage attached to the camera window. Fig. 10 shows a schematic view of the XY-scanner. This module has eight UV LEDs (NICHIA-NSHU590B) with a wavelength of 365 nm ± 10 nm (FWHM). Each UV LED has an attached plane-convex lens to ensure the light is parallel and produces a spot size of 4 mm in diameter. The XY-scanner's moving arm has a vertical range of 890 mm and a horizontal range of 1040 mm. This allows it to completely sweep over the camera's photon sensitive area. The design accuracies are as follows:

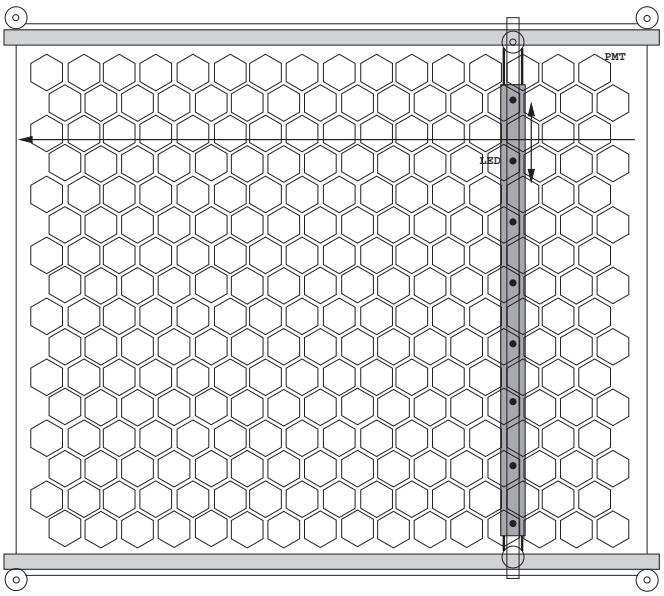

Fig. 10. The schematic view of the XY-scanner. The covering area of each LED is 2.5 PMTs vertically and 16 PMTs horizontally.

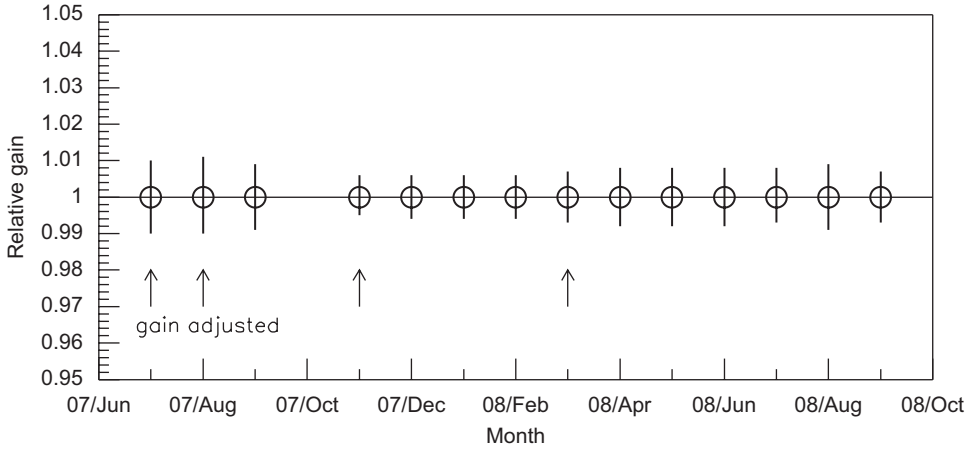

Fig. 9. The variation of a relative gain of a PMT through all the observation periods.

mounting point: ±1.0 mm, movement: ±0.05 mm, and holding: ±0.5 mm. Considering these accuracies are much smaller than the light source spot size, we can accurately obtain non-uniformity measurements. We measured the non-uniformities of the cameras after their installation. This was done in order to avoid any position dependencies, such as effects due to the terrestrial magnetic field.

The specifications for LED light pulses are as follows: pulse width: 400 ns, light intensity: ~1000 p.e., and pulse repetition frequency: 4 kHz. The intensity fluctuation is less than ±2%, as shown in Fig. 11. The XY-scanner has eight UV light sources that independently illuminate eight different points. This greatly reduces to time spent taking non-uniformity measurements. These light sources are attached to the moving arm at even intervals in a vertical line. The number of measurement points per PMT is about 200 with 4 mm spacing. Data from 60 UV LED shots are recorded for each point. When non-uniformity measurements are made, the XY-scanner has adjacent UV LEDs map out the same area of the camera. This allows us to determine the relative intensities of the UV LED sources. In order to save time, this overlap area is restricted to a vertical height of half the PMT diameter.

The uncertainty of each light intensity is within ±1% (1σ). The largest estimated error of the relative light intensity between LED #1 and LED #8 is 2% (1σ), which is produced by summing the uncertainties from all the LEDs.

With the XY-scanner, it takes 3 h to take non-uniformity measurements for the whole camera.

The light intensities of the UV LED sources vary during measurement because of changing temperature. Thus, we monitor the intensities of the UV LEDs by measuring a point on a PMT and then measuring the same point again 10 min later. The intensity variations are corrected using this monitoring data. Fig. 12 shows the light intensity of an LED from camera #05 at the BR station. In this case, the intensity is stable to within 1% (1σ).

Fig. 13 shows the non-uniformity of 253 PMTs for camera #05 at the BR station. It should be noted that data from three standard PMTs are excluded because YAP is mounted over them.

Fig. 14 consists of two plots which are the x and y axis cross-sections of the plots found in Fig. 13. The relative response strength within a circle of radius r mm is shown in Fig. 15. Here,

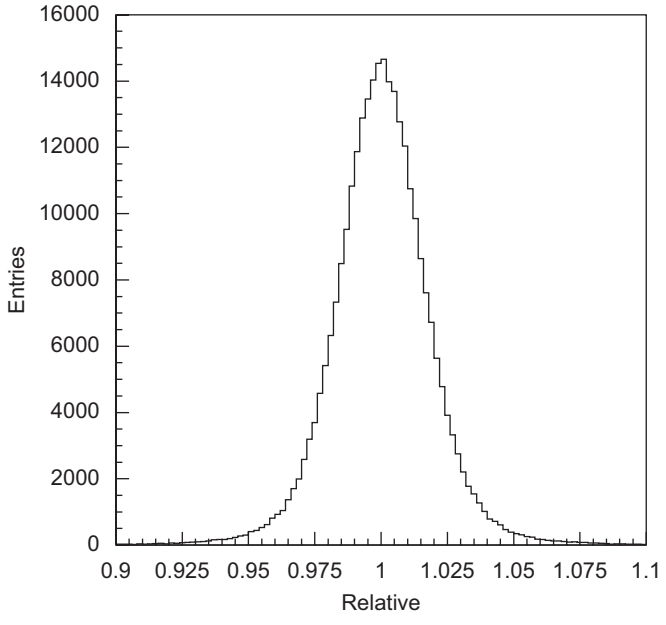

Fig. 11. The typical intensity fluctuation of an LED (LED #1).

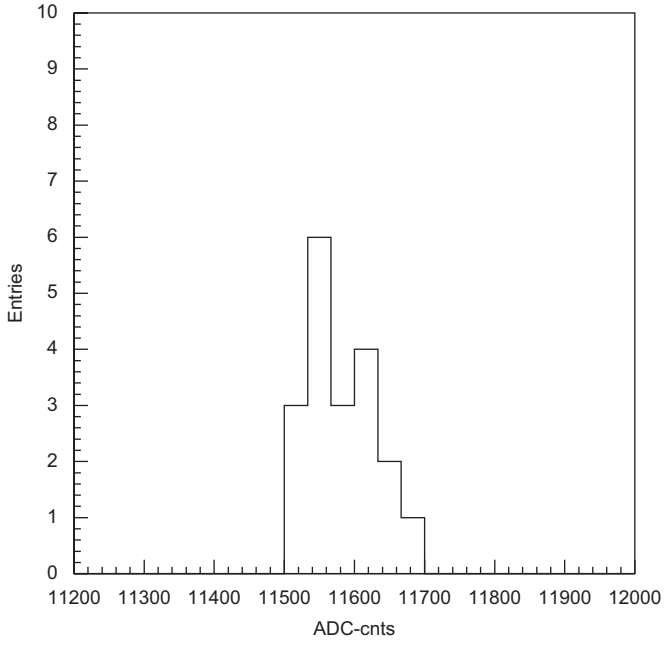

Fig. 12. The typical stability of the LED light intensity of camera #05 at the BR station during a measurement.

the circle involving 90% of total response is defined as the sensitive region (error bars: 1σ). From the average, the radius of the sensitive region is 28.4 mm ± 0.3 mm, and the individual difference of region size is 2%. The ratio of the sensitive region to the total area of the PMT head is 89%. Additionally, the ratio of the sum of 256 PMTs' sensitive area to the geometrical focal plane area of a camera is 83%.

From our preliminary simulations, the non-uniformities cause the systematic error of the energy estimation to rise 4%. However, we can eliminate this increasing systematic error using these measured non-uniformities. Now we are developing a precise FD-simulator, and estimating the total systematic error of FD analysis. The details will be provided in forthcoming publications.

6. Summary

The FDs of TA are calibrated methodically. The applied voltages for the absolutely calibrated PMTs are determined through calibration with CRAYS. Three absolutely calibrated PMTs are mounted on each camera. The Xe flasher is used for relative calibration. Essentially, the high voltages to the PMT are adjusted until its gain equals the absolutely calibrated PMT gain.

Moreover, the gains of the absolutely calibrated PMTs are monitored by continuous illuminations with the YAP pulser. Relative gains of all the PMTs are measured using the Xe flasher once every hour during observations. For one year, PMT output responses are stable within 3% standard deviation. Non-uniformities of PMT photo cathodes and gaps between PMTs are measured with the XY-scanner. This is done on site, after the camera has been installed. The individual differences of non-uniformities are small compared with measurement errors. These measured non-uniformities eliminate systematic error of the energy estimation.

For precise estimations of primary energies of EASs, we need to know atmospheric transparency, fluorescence photon yields and other atmospheric conditions at the exact moment of the event. In order to monitor atmospheric transparencies, we installed an LIDAR (Light Detection And Ranging) system [16], and a laser facility between the three FD stations [18].

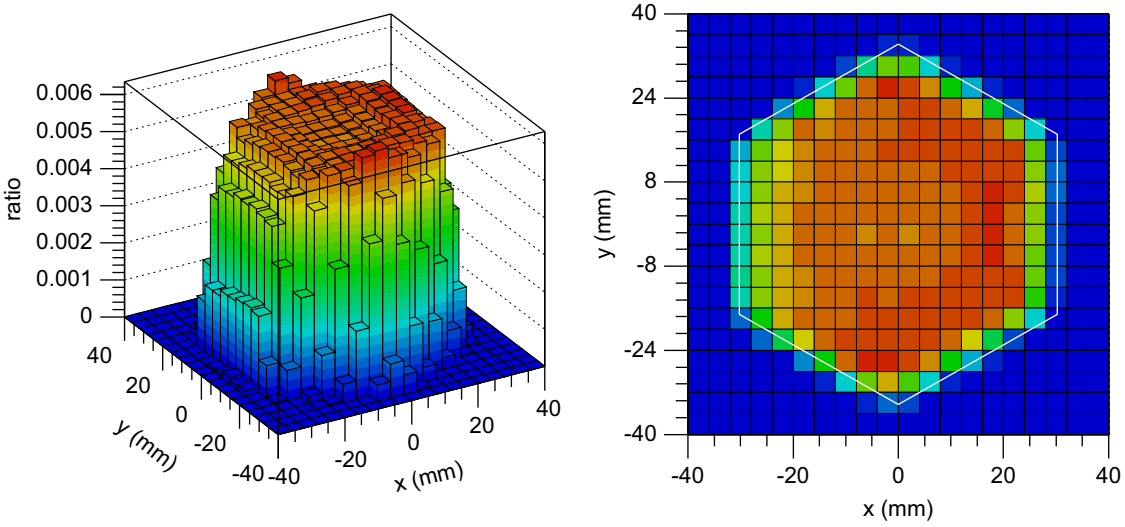

Fig. 13. The non-uniformity of the photo cathodes on camera #05 at the BR station (plots: median value of 253 PMTs).

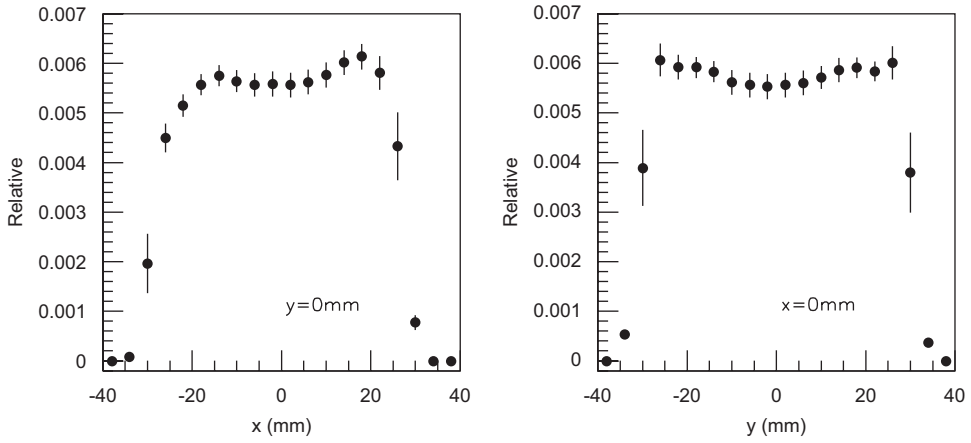

Fig. 14. The cross-sectional views of Fig. 13 along the x and y axes (plots: median value of 253 PMTs, error bars: 1σ).

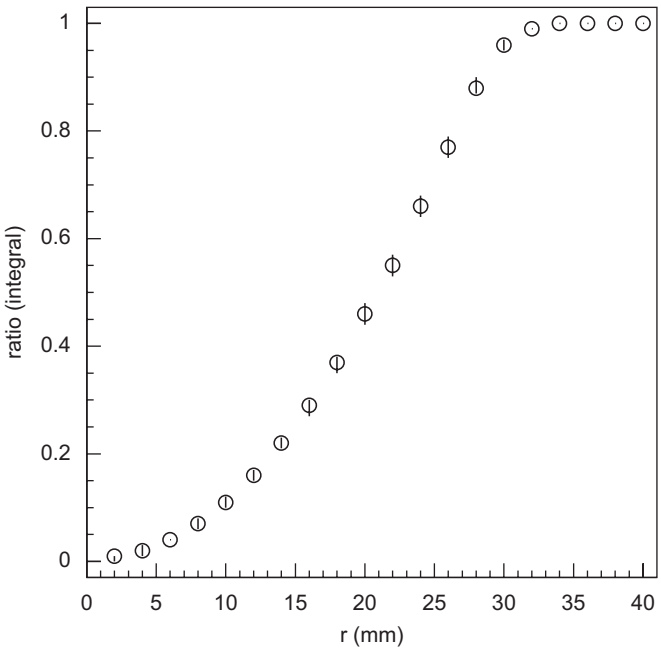

Fig. 15. The relative response strength of PMT within a circle of radius r mm.

Additionally, we will install an electron linear accelerator in front of the BR station for end to end calibrations [17]. In analysis, the atmospheric conditions are monitored in two different ways. First, measurements of the temperature, humidity, and pressure are taken by the various sensors installed in the FD stations. Second, radiosonde observations are launched twice a day from Salt Lake City [22]. The information gathered by these separate means are collaboratively used to adjust the atmospheric correction factors.

Acknowledgments

The Telescope Array experiment is supported by the Ministry of Education, Culture, Sports, Science and Technology, Japan, Grant-in-Aid for Scientific Research on Priority Areas, "The Origin of the Highest Energy Cosmic Rays", 2003, and for Scientific Research (B), 20340057, 2008. This experiment is also supported by the US National Science Foundation (NSF) through awards PHY-0307098 and PHY-0601915 (University of Utah) and PHY-0305516 (Rutgers University). The Dr. Ezekiel R. and Edna Wattis Dumke Foundation, The Willard L. Eccles Foundation, and The George S. and Dolores Dore Eccles Foundation all helped with generous donations. The State of Utah supported the project through its Economic Development Board, and the University of Utah supported us through the Office of the Vice President for

Research. The use of the experimental site became possible by the cooperation of the State of Utah School and Institutional Trust Lands Administration (SITLA), the federal Bureau of Land Management (BLM), and the United States Air Force. We also wish to thank the people and the officials of Millard County, Utah, for their steadfast and warm supports. H.T. and U.T. was supported by a 21st Century COE program by the Ministry of Education, Culture, Sports, Science and Technology at University of Tokyo "Quantum Extreme Systems and Their Symmetries" and at Tokyo institute of Technology "Nanometer-Scale Quantum Physics", respectively. D.I. was supported by Grants-in-Aid for JSPS Fellows. We gratefully acknowledge the contributions from the technical staffs of our home institutions. The authors acknowledge Prof. John N. Matthews, and Mr. Zachary Zundel of University of Utah, for providing many useful comments. We thank HAMAMATSU Photonics K.K. for their kindly support.

References

[1] K. Greisen, Phys. Rev. Lett. 16 (1966) 748;
T. Zatsepin, V.A. Kuzmin, JETP Lett. 4 (1966) 178.
[2] J. Linsley, J. Phys. G 12 (1986) 51.
[3] M.M. Winn, et al., J. Phys. G 12 (1986) 653.
[4] M.A. Lawrence, R.J.O. Reid, A.A. Watson, J. Phys. G 17 (1991) 51.
[5] M. Nagano, et al., J. Phys. G 18 (1992) 423;
S. Yoshida, et al., Astropart. Phys. 3 (1995) 105.
[6] D.J. Bird, et al., Astrophys. J. 424 (1994) 491.
[7] V.P. Egorova, et al., Nucl. Phys. B (Proc. Suppl.) 136 (2004) 3.
[8] M. Takeda, et al., Astropart. Phys. 19 (2003) 447.
[9] R.U. Abbasi, et al., Phys. Rev. Lett. 100 (2008) 101101.
[10] J. Abraham, et al., Phys. Rev. Lett. 101 (2008) 061101.
[11] H. Kawai, et al., Nucl. Phys. B (Proc. Suppl.) 175–176 (2008) 221.
[12] N. Sakurai, et al., in: Proceedings of the International Cosmic Ray Conference, 2007.
[13] J. Matthews, et al., in: Proceedings of the International Cosmic Ray Conference, 2007.
[14] Y. Tsunesada, et al., in: Proceedings of the International Cosmic Ray Conference, 2007.
[15] H. Tokuno, et al., in: Proceedings of the International Cosmic Ray Conference, 2007.
[16] M. Chikawa, et al., in: Proceedings of the International Cosmic Ray Conference, 2007.
[17] T. Shibata, et al., Nucl. Instr. and Meth. A 597 (2008) 61.
[18] S. Udo, et al., in: Proceedings of the International Cosmic Ray Conference, 2007.
[19] C. Rozsa, et al., in: IEEE Nuclear Science Symposium, 1999.
[20] M. Kobayashi, et al., Nucl. Instr. and Meth. A 337 (1994) 355.
[21] M. Kobayashi, et al., KEK Internal 91-1, 1991.
[22] S. Machida, et al., in: Proceedings of the International Cosmic Ray Conference, vol. 8, 2005, p. 169.